JOM, Vol. 69, No. 9, 2017
DOI: 10.1007/s11837-017-2439-y

DC Electric Arc Furnace Application for Production of Nickel-Boron Master Alloys

MURAT ALKAN,[1,4] KEREM CAN TASYÜREK,[2] MEHMET BUGDAYCI,[2,3] AHMET TURAN,[3] and ONURALP YÜCEL[2]

1.—Department of Metallurgical and Materials Engineering, Faculty of Engineering, Dokuz Eylül University, 35397 Buca, Izmir, Turkey. 2.—Metallurgical and Materials Engineering Department, Faculty of Chemical and Metallurgical Engineering, Istanbul Technical University, 34469 Maslak, Istanbul, Turkey. 3.—Chemical and Process Engineering Department, Faculty of Engineering, Yalova University, 77100 Yalova, Turkey. 4.—e-mail: alkan.murat@deu.edu.tr

In this study, nickel-boron (Ni-B) alloys were produced via a carbothermic reduction starting from boric acid (H_3BO_3) with high-purity nickel oxide (NiO), charcoal, and wood chips in a direct current arc furnace. In electric arc furnace experiments, different starting mixtures were used, and their effects on the chemical compositions of the final Ni-B alloys were investigated. After the reduction and melting stages, Ni-B alloys were obtained by tapping from the bottom of the furnace. The samples from the designated areas were also taken and analyzed. The chemical composition of the final alloys and selected samples were measured with wet chemical analysis. The Ni-B alloys had a composition of up to 14.82 mass% B. The phase contents of the final alloys and selected samples were measured using x-ray diffraction (XRD). The XRD data helped predict possible reactions and reaction mechanisms. The material and energy balance calculations were made via the XRD Rietveld and chemical compositions. Nickel boride phases started to form 600 mm below the surface. The targeted NiB phase was detected at the tapping zone of the crucible (850–900 mm depth). The energy consumption was 1.84–4.29 kWh/kg, and the electrode consumption was 10–12 g/kg of raw material charged.

INTRODUCTION

Nickel-based alloys have wide use in high-temperature applications, in metallurgical applications requiring corrosion and wear resistance, and within energy industries such as for turbine blades and parts.[1,2] Although there have been various studies on nickel-boron (Ni-B) coatings, there are few reports on Ni-B alloy production. Ni-B coatings are useful for the aerospace, automotive, and electronic industries because they are hard and wear/corrosion resistant.[3] Solids containing Ni-B can also be used as a catalyst.[4]

Ni-B alloys are an alternative coating material to the expensive noble metals. Ni-B electroplated coatings have lower resistivity and low-current sliding contacts than other noble metals, while having higher wear resistance and hardness properties.[5] Rajagopal[6] compared the properties of the electrodeposited and electroless coated Ni-B alloys via their compositions, solderability, tensile strength, hardness, corrosion, and abrasion resistance as determined via x-ray diffraction (XRD), microstructure, and differential thermal analysis (DTA) techniques. The structural properties of Ni-B coatings depend on the boron content and deposition conditions. For example, the application of heat treatment can result in an excessive increase in the hardness of the coating.[7] Both electroless and electrolytic coatings can be used for the Ni-B alloys' applications on various substrates like steel, aluminum alloys, magnesium alloys, and ceramics.[3–11]

Besides the coating processes, Ni-B alloys can also be produced by mechanical alloying, sol–gel, or reduction methods. Corrias et al.[12] studied the production of Ni-B nanocrystalline powders via ball milling powder metallurgy (P/M) technique. They investigated the phase formations during the milling process. At a Ni:B molar ratio of 4:1, the Ni, Ni_3B and amorphous phases were detected.

Meanwhile, the Ni_2B phase formed at a 3:2 Ni:B molar ratio. Fadeeva et al.[13] studied the production of Ni-B alloys having 5 at.% and 13 at.% B by mechanical alloying. They investigated the structural properties and solid solution abilities of the alloys. Peng et al.[14] studied the production of Ni-B alloy powders using an electrochemical reduction method from molten salt mixtures. The starting mixtures with different Ni/B ratios were prepared via sol–gel methods followed by heat treatment. The powder products consisted of a mixture of Ni_3B, Ni_2B, and Ni.

Direct current (DC) arc furnaces have been used for more than 40 years in ferrous and nonferrous industries. DC arc furnaces have several advantages over alternating current (AC) arc furnaces: decreased emission of out-gasses and ambient noise, controlled melting processes and metal compositions, and decreased power and energy consumption.[15] DC arc furnaces also do not have any backlashing of the arc (generation of arc repulsion can be prevented with a single electrode system). This can prevent the formation of hot spots.[16]

The first application of a carbothermal method producing Ni-B alloys with an electric arc furnace composition was realized in 1986. Hahn et al.[17] produced nickel-boron alloys starting from mixtures of boric acid, metallic nickel chips from a nickel cathode, wood charcoal, and wood chips. Metallic nickel chips were used as nickel sources, and the studies were realized in a three-electrode arc furnace.

In this study, the carbothermic reduction of H_3BO_3:NiO (boric acid:nickel oxide) mixtures were studied with a DC single-electrode submerged electric arc furnace (EAF). A carbothermic reduction including an electric arc furnace enables industrial-scale production. The DC arc furnace was selected because of its advantages over an AC arc furnace. The reaction behaviors of reduction processes were investigated, and the reaction mechanisms were predicted for each selected zone. The compositions of the final alloys and by-products obtained from each zones were measured, as were the reaction and energy efficiencies.

EXPERIMENTAL PROCEDURE

In experimental studies, a mixture of granulated boric acid (H_3BO_3) and technical-grade green nickel oxide (NiO) with charcoal and wood chips were used to obtain a Ni-B master alloy. The H_3BO_3 and NiO have purities of 99.5 wt.% and 99.0 wt.%, respectively, with an average grain size of 0.5 mm. The impurities in NiO are Co_3O_4, MgO, SiO_2, CaO, Na_2O, and Fe_2O_3 with concentrations of 450 ppm Co, 200 ppm Mg, 110 ppm Si, 90 ppm Ca, 80 ppm Fe, and 80 ppm Na. The H_3BO_3 was bought from Eti Mine Inc., and it has 300 ppm SO_4, 5 ppm Cl, and 5 ppm Fe. Three different charcoals were used as reductants, and wood chips were used for gas permeability. The grain sizes of the charcoal and wood chips were 1–3 mm and 5–20 mm, respectively. Chemical analysis of charcoal and wood chips is provided in the online supplementary material in Table SI. The ash in charcoal #2 is 47.5% SiO_2, 12.18% Fe_2O_3, 10.65% CaO, 23.90% Al_2O_3, and 4.48% MgO by mass.

The carbothermic reactions were realized in a 270-kVA DC electric arc furnace with a single electrode. The graphite-lined EAF has a charge capacity of 250 kg. The inner diameter of the furnace was 360 mm and has 900 mm depth. The schematic view of EAF was given in the online supplementary material in Fig. S1.

The raw mixtures were prepared to produce 15 mass% B-containing Ni-B master alloy using a mixture of H_3BO_3/NiO with a mass ratio of 1.0/1.3. The mass ratio of wood chips in the mixtures was fixed as 15.0 mass%. The mass ratio of the total fixed carbon amount into the raw mixtures was also fixed as 13.0 mass% while using different types of charcoal. These mixture values were chosen based on previous studies.[18] The amount of initial mixtures used here is given in the online supplementary material in Table SII.

The electric arc strike was ignited, and the furnace was preheated before charging the raw materials. A preheating session was applied to heat the graphite linings, control the arc strike, and elevate the electrode. The preheating session ran for 60 min, and the arc strike was then stopped. After the preheating session, the lower part of the furnace linings reached 250°C. First, 20 kg of raw materials were charged into the crucible. After that, the arc was ignited again, and the rest of the mixture was added manually at 1 kg/min. The voltage, current, and energy consumption values were measured manually. The temperature measurements during reaction and tapping of the alloy were done using an optical pyrometer. The furnace off-gas was sent into a single-bagged bag filter. The off-gas composition was not studied here. At the end of the experiments, the liquid metal was tapped from the bottom and the arc was stopped. The furnace was left to cool. After cooling, the by-product samples were taken into five different zones (every 200 mm depth of the furnace). These resulting samples are called by-products, and these are a mixture of unreacted and reacted materials (mixture of slag, alloy, and dross). After cooling, by-product samples were removed with a chisel and hammer. The master alloys and by-products were characterized by wet chemical analysis methods and XRD technique (RIGAKU MiniFlex with Cu K_α anode).

RESULTS AND DISCUSSIONS

Energy Consumptions

The results are given in the online supplementary material in Table SIII. As a result of the higher amount of raw materials, the feeding and reaction of

Table I. Energy and electrode consumption values of the experiments

	Energy consumption			Electrode consumption			
Exp. no.	kWh	kWh/kg raw mat.	kWh/kg alloy	g	g/kg raw mat.	g/kg alloy	g/h
RUN 1	147.46	1.84	13.05	904.2	11.29	80.02	4.46
RUN 2	213.84	2.14	26.40	1239.3	12.39	153.00	4.66
RUN 3	120.97	3.02	23.72	469.9	11.75	92.14	3.42
RUN 4	171.50	4.29	38.11	400.0	10.00	88.89	4.12

Table II. Chemical analysis results of the Ni-B Master alloys obtained after tapping

	Compositions, mass percent								
Exp. no.	Ni	B	Al	S	Si	Fe	C	P	Expected phases
RUN 1	89.02	9.94	0.16	0.137	0.36	0.18	0.18	0.018	Ni_3B, Ni_4B_3 (Ni_2B, Ni_3B_2)
RUN 2	83.11	14.82	0.33	0.012	0.37	0.25	1.08	0.013	NiB, Ni_4B_3
RUN 3	82.85	14.62	0.07	0.005	0.80	0.19	0.92	0.015	NiB, Ni_4B_3
RUN 4	85.02	13.35	0.09	0.002	0.42	0.31	0.25	0.020	NiB, Ni_4B_3

RUN 1 and RUN 2 lasted for more than 90 min. The highest energy consumption value was obtained in RUN 2. The energy consumption values were calculated based on the amount of both raw materials charged and master alloys acquired. The energy-to-mass ratios of the raw materials were obtained as 1.84 kWh/kg, 2.13 kWh/kg, 3.02 kWh/kg, and 4.29 kWh/kg raw materials, respectively. The energy-to-mass ratios of the master alloys were 13.05 kWh/kg, 26.40 kWh/kg, 23.72 kWh/kg, and 38.11 kWh/kg product, respectively. The power-to-weight ratios of the raw materials were calculated as 2.91 kW/kg, 3.20 kW/kg, 3.52 kW/kg, and 2.85 kW/kg, respectively. The highest power consumption was realized where charcoal #2 was used as the reductant. This is because of the lower fixed carbon and higher ash content in its composition. The detailed energy and electrode consumption values of the experiment are provided in Table I.

The energy consumption values given in Table I are the sum of both the preheating and reduction stages. As a result of the longer preheating time, the energy consumption value in RUN 4 was the highest. The electrode consumption rate also decreased with increased fixed carbon content in the charcoal.

The theoretical energy requirements of the experiment were calculated using the "Reaction" module of FactSage™ 6.4 "The Integrated Thermodynamic Databank System."[19] The total theoretical energy requirements (used for reducing and melting the products) were estimated as 82.2 kWh, 127.3 kWh, 51.8 kWh, and 53.7 kWh, respectively. The ratios of energy losses during the experiments were 44.3%, 40.5%, 57.2%, and 68.7%, respectively. The energy was lost as a result of the preheating stage.

Chemical Compositions

The chemical analysis results of the master alloys are given in Table II. The impurity contents of the alloys were within the limitation values of the ASTM A323-05 ferro-boron standard specification. The B content in RUN 1 was obtained at lower values as a result of the higher amount of unreacted materials. The expected phases were detected via the Ni-B binary phase diagram given in Fig. 1.

The Ni-B phase diagram given in Fig. 1 was plotted using the "Phase Diagram" module of the FactSage™ 6.4 "BINS" database.[19] All alloys obtained from the experiments except RUN 1 have the same cooling regime. The XRD analysis of the master alloy by RUN 2 is given in the online supplementary material in Fig. S2. The final alloy composition contained both NiB and Ni_4B_3 phases, which have the lowest melting temperature in the Ni-B binary phase diagram (Fig. 1). The XRD results of the casting alloys match with the binary phase diagram. The NiB and Ni_4B_3 phases were detected in RUN 2, RUN 3, and RUN 4, whereas the Ni_2B and Ni_4B_3 phases were detected in RUN 1.

Reaction Mechanisms

To understand the possible mechanism of nickel-boron formation, samples from specified areas were taken and analyzed. The comparative XRD analysis result of the samples taken from RUN 2 at different reaction zones is given in Fig. 2.

There are three possible reactions for complete reduction of NiO into Ni via a carbon-containing source. The reduction of boric acid into metallic boron is realized via two steps: dehydration of boric acid (obtaining boron oxide) and carbothermal reduction. The thermodynamic reactions of the

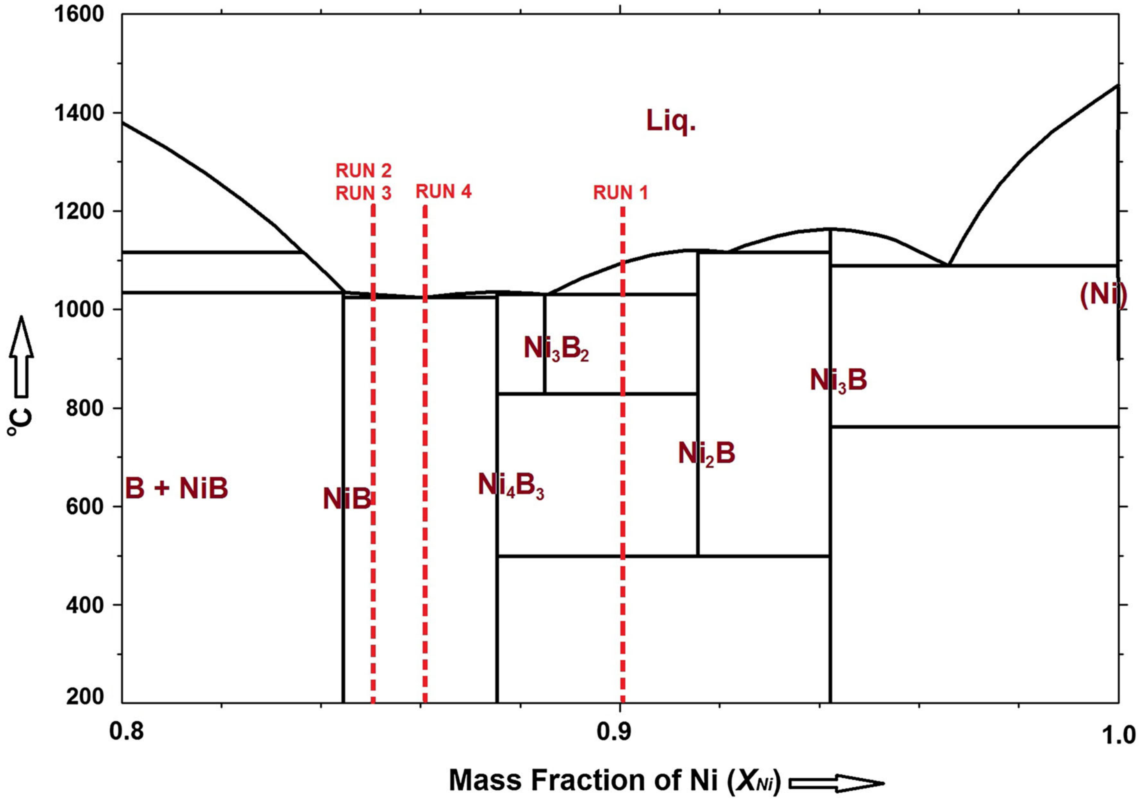

Fig. 1. Ni-B phase diagram plotted via the phase diagram module and BINS database of FactSage^{TM} 6.4.

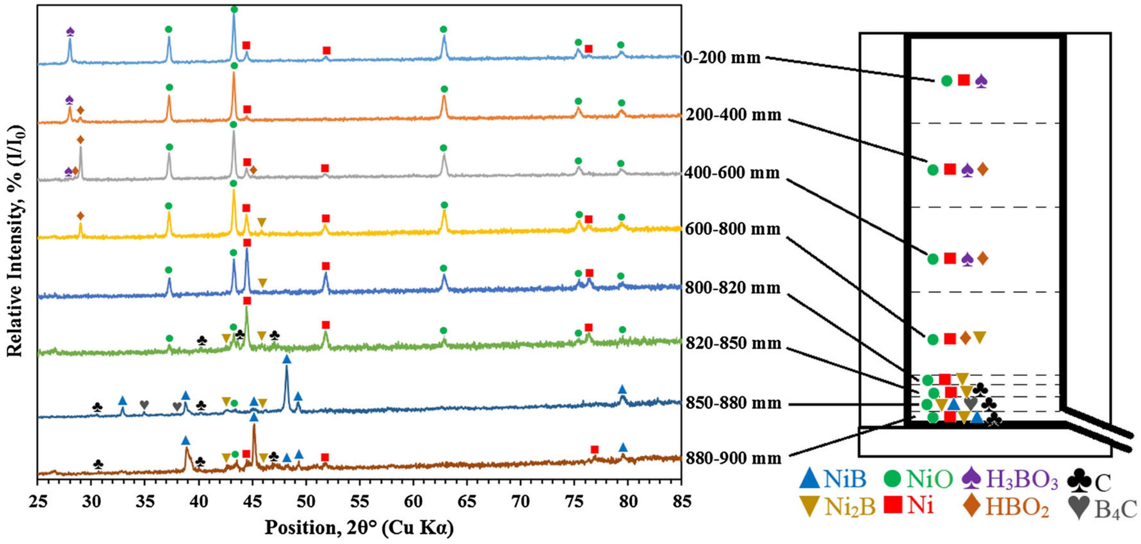

Fig. 2. Comparative XRD analysis results of by-product samples taken from the selected zones in RUN 2.

NiO-H_3BO_3-C system between 0°C and 2000°C are given as follows (remaining reactions are not thermodynamically feasible):

$$NiO + C = Ni + CO_{(g)} \tag{1a}$$

$$NiO + 0.5C = Ni + 0.5\ CO_{2\,(g)} \tag{1b}$$

$$NiO + CO_{(g)} = Ni + CO_{2\,(g)} \tag{1c}$$

$$H_3BO_3 + Q_{(heat)} = HBO_2 + H_2O \tag{2a}$$

$$H_3BO_3 + Q_{(heat)} = 0.5\ B_2O_3 + 1.5\ H_2O \tag{2b}$$

$$HBO_2 + Q_{(heat)} = 0.5B_2O_3 + 0.5\ H_2O \tag{2c}$$

$$H_3BO_3 + 1.5\ C = B + 1.5\ CO_{(g)} + 1.5\ H_2O \tag{3a}$$

$$H_3BO_3 + 0.75C = B + 0.75\ CO_{2\,(g)} + 1.5\ H_2O \tag{3b}$$

$$HBO_2 + 1.5\ C = B + 1.5\ CO_{(g)} + 0.5\ H_2O \tag{3c}$$

$$B_2O_3 + 3C = 2B + 3CO_{(g)} \tag{3d}$$

$$Ni + B = NiB \tag{4a}$$

$$Ni + 0.5\ B = 0.5\ Ni_2B \tag{4b}$$

$$Ni + 0.33\ B = 0.33\ Ni_3B \tag{4c}$$

$$Ni + 0.75\ B = 0.25\ Ni_4B_3 \tag{4d}$$

$$Ni + 0.66\ B = 0.33\ Ni_3B_2 \tag{4e}$$

$$C + 4\ B = B_4C \tag{5a}$$

$$C + CO_{2(g)} = 2CO_{(g)} \tag{5b}$$

$$C + 0.5O_{2(g)} = CO_{(g)} \tag{5c}$$

$$C + O_{2(g)} = CO_{2(g)} \tag{5d}$$

The standard Gibbs free energy of formation of the given reactions varies with increasing temperature and was plotted using the "Reaction" module of FactSage^{TM} 6.4 and shown in the online supplementary material in Fig. S3. As observed in Fig. 2, the formation of metallic Ni was realized even on the top of the crucible. The ratio of relative intensity of Ni to NiO increased in deeper parts of the furnace. The reduction of NiO into metallic Ni was dependent on the existence of $CO_{(g)}$ at lower temperatures. Nevertheless, according to the Boudouard Reaction (Eq. 5b) and Fig. S3a in the online supplementary material, $CO_{2\ (g)}$ is more stable than $CO_{(g)}$ at temperatures below 700°C. Thus, the source of $CO_{(g)}$ that was used as a reducing agent for NiO was generated on the lower and hotter parts of the furnace. The gas permeability of the green mixture let $CO_{(g)}$ diffuse through the top of furnace. Equation 1a becomes more feasible than Eq. 1c just over 700°C (Fig. S3a). But, direct reduction of NiO by carbon could be possible at the temperature where Eq. 1a is more feasible than Eq. 5c. The reduction of NiO by carbon (Eq. 1a) could only be realized over 2460°C. At temperatures below 2460°C, carbon was burnt with oxygen to form $CO_{2\ (g)}$ (Eq. 5d). Then, $CO_{(g)}$ was generated via Eq. 5b, and NiO was reduced by $CO_{(g)}$ via Eq. 1c to produce metallic Ni.

Boric acid (H_3BO_3) was used as a boron source, and it can be easily dehydrated even at lower temperatures (Fig. S3b in the online supplementary material). With increasing temperature, the HBO_2 phase was expected to form first and then the B_2O_3 phase could be obtained according to Eqs. 2b and 2c. Despite the dehydration process, the reduction of boron sources into elemental boron can be realized at higher temperatures (Fig. S3c). As a result of the thermodynamic calculations, Eqs. 3a, 3c, and 3d can only be feasibly at temperatures over 1350°C, 1520°C, and 1620°C, respectively. The reduction mechanism of the boron sources into the elemental boron was carbothermic, and it was dependent on the carbon content in the charge. According to the thermodynamic data, the reduction of any boron sources by $CO_{(g)}$ is not possible between 0°C and 2000°C.

Figure S3d in the online supplementary material shows that the formation of nickel borides (NiB, Ni_2B, Ni_3B, $N_{i4}B_3$, and Ni_3B_2) is feasible between these temperatures. The production of B_4C, even at a lower grade, can also be thermodynamically feasible in the presence of both elemental boron and carbon. Nickel-boride phases started below 600 mm, especially in the area under the top electrode. The NiB phase (theoretically, composition of NiB contains 15.5 mass% boron) was obtained in the tapping zone areas between 850 mm and 900 mm depth. Also, B_4C formed as a result of the higher temperatures around the electrode.

The possible phases and amounts of products were simulated using the "Equilib" module of FactSage^{TM} 6.4. In this module, the Gibbs energy minimization method is used.[19] Here, FactPS, FToxide, SGTE (2014), and BINS databases were selected for calculations, and conflicts were collated manually. Thus, the results were given based on the most probable reactions in the selected conditions. The amount of possible products resulting from the increasing temperature for RUN 2 is given in the online supplementary material in Fig. S4. Figure S4 was plotted based on the results of thermodynamic calculations in the starting mixture containing 28.7 kg of technical grade of nickel oxide, 37.4 kg of granulated boric acid, 19.6 kg of charcoal (#2), and 14.3 kg of wood chips. All compounds and impurities in the starting mixture were included in the calculations.

Figure S4a in the online supplementary material shows that the reduction of NiO into metallic Ni started at just over 100°C, whereas dehydration of H_3BO_3 into HBO_2 was realized at room temperature despite the fact that NiO and HBO_2 can be completely consumed at temperatures below 200°C and 600°C, respectively. According to the XRD results (Fig. 2), the H_3BO_3, and HBO_2 phases were detected up to 600 mm and 800 mm, respectively, whereas Ni and NiO were detected in all zones of the

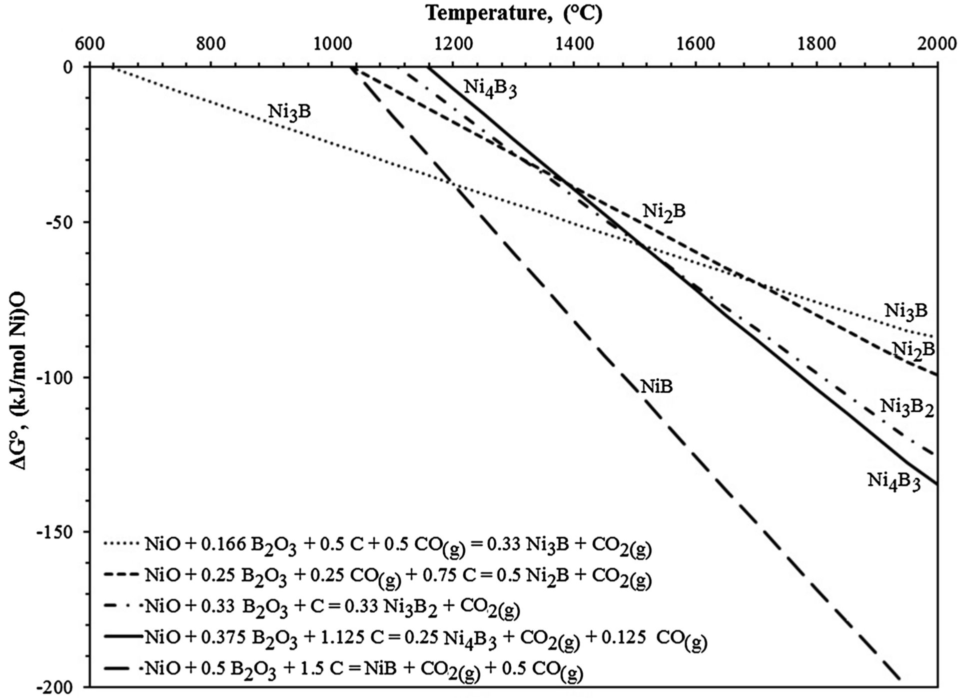

Fig. 3. Standard Gibbs free energy of formation values of the possible reactions for production of nickel borides.

furnace. This suggests that the temperature changes in every zone of the furnace and should not be homogenous. The hot gases that were generated at the deeper zones of the furnace (around the electrodes) should increase the local temperature in the shallower zones.

Figure S4a and b in the online supplementary material showed that the amount of gaseous phases increased while the temperature increased. B_2O_3 in SLAG phase was reacted with water vapor, and a gaseous HBO_2 phase was generated. Consequently, the formation of HBO_2 gasses, metallic boron, and nickel boride phases cannot be obtained theoretically even at higher temperatures. The formation of nickel borides could be explained by the reaction of glassy boric oxide (B_2O_3) with unreacted carbon (C) and reduced Ni from the reaction of NiO and $CO_{(g)}$. The "Equilib" module assumed that all of the elemental carbon was burnt with oxygen to form $CO_{(g)}$, but in fact the C was not totally burnt. The possible reactions for producing of nickel borides are the sum total of Eqs. 1c and 3d with Eq. 4a (Eqs. 4b, 4c, 4d, or 4e). The standard Gibbs free energy changing of formation of nickel borides is given in Fig. 3, and the total reactions are suggested as:

$$\mathrm{NiO} + 0.5\mathrm{B_2O_3} + 1.5\ \mathrm{C} \ = \ \mathrm{NiB} + 0.5\ \mathrm{CO_{(g)}} + \mathrm{CO_{2(g)}} \tag{6a}$$

$$\begin{aligned}&\mathrm{NiO} + 0.25\ \mathrm{B_2O_3} + 0.75\ \mathrm{C} \ + 0.25\ \mathrm{CO_{(g)}}\\ &\quad = \ 0.5\ \mathrm{Ni_2B} \ + \mathrm{CO_{2(g)}}\end{aligned} \tag{6b}$$

$$\begin{aligned}&\mathrm{NiO} + 0.166\ \mathrm{B_2O_3} + 0.5\ \mathrm{C} \ + 0.5\ \mathrm{CO_{(g)}}\\ &\quad = \ 0.333\ \mathrm{Ni_3B} \ + \mathrm{CO_{2(g)}}\end{aligned} \tag{6c}$$

$$\begin{aligned}&\mathrm{NiO} + 0.375\ \mathrm{B_2O_3} + \ 1.125\ \mathrm{C}\\ &\quad = \ 0.25\ \mathrm{Ni_4B_3} + 0.125\ \mathrm{CO_{(g)}} + \mathrm{CO_{2(g)}}\end{aligned} \tag{6d}$$

$$\mathrm{NiO} + 0.333\ \mathrm{B_2O_3} + \mathrm{C} = 0.333\ \mathrm{Ni_3B_2} + \mathrm{CO_{2(g)}} \tag{6e}$$

Nickel oxide was reduced to metallic Ni by $CO_{(g)}$ (Eq. 1c), whereas boron oxide was reduced to elemental B by C (Eq. 3d); NiB was synthesized by the reaction between Ni and B (Eq. 4a). These three reactions were summarized as a single reaction (Eq. 6a), and Fig. 3 shows that the synthesis of NiB can be thermodynamically possible over 1050°C. Accordingly, the temperature in the deeper areas of the furnace should be higher than 1050°C. At temperatures between 600°C and 1050°C, Ni_3B is the only stable nickel boride, and it contains only 6 mass% of boron. As the temperature increases, NiB will become the most stable compared with other nickel borides. NiB is the highest boron-containing nickel boride, and the composition of NiB consists of more than 15 mass% of boron. Therefore, for production of higher boron-containing Ni-B alloys, the working temperature must be higher than at least 1200°C.

The temperature measurement of the final alloys during melting and electrode surface functionalization used an optical pyrometer. The temperature of the melted alloys were measured between 1145°C

Table III. Compounds in the by-products detected via XRD technique taken from selected areas and a list of possible formation reactions

Reaction zone (mm)	Detected phases and possible formation reactions			
	RUN 1	**RUN 2**	**RUN 3**	**RUN 4**
600–800	NiO, Ni, C Equations 1c , 2c	NiO, Ni, HBO_2, Ni_2B Equations 1c, 2a, and 6b	NiO, Ni, HBO_2, H_3BO_3 Equations 1c , 2a	NiO, Ni Equations 1c , 2c
800–820	NiO, Ni Equations 1c and 2c	NiO, Ni, Ni_2B Equations 1c, 2c, and 6b	NiO, Ni Equations 1c and 2c	NiO, Ni, C Equations 1c , 2c
820–850	NiO, Ni, Ni_2B, C Equations 1c, 2c, and 6b	NiO, Ni, Ni_2B, C Equations 1c, 2c, and 6b		
850–880	Ni, Ni_2B, C Equations 1c, 2c, and 6b	Ni, NiB, Ni_2B, C, B_4C Equations 1c, 2c, 5a, 6a, and 6b	NiB, Ni, C Equations 1c, 2c, and 6a	NiO, Ni, NiB, C Equations 1c, 2c, 6a
880–900	Ni, Ni_2B, C Equations 1c, 2c, and 6b	NiO, Ni, NiB, Ni_2B, C Equations 1c, 2c, 6a, and 6b	NiB, NiO, Ni, C Equations 1c, 2c, and 6a	NiB, Ni_2B, Ni, C Equations 1c, 2c, 6a, and 6b

and 1275°C during tapping. The temperature measured on the surface of the electrode was between 680°C and 720°C. The temperature profile of the furnace could not be measured with an optical pyrometer, but it could be estimated via the XRD results (Fig. 2) and possible phases obtained at different temperatures (Figs. S3, S4, and Fig. 3). The projected temperature profile of the furnace during the RUN 2 process was given in the online supplementary material in Fig. S5. The minimum and maximum temperatures were selected because of the stability ranges of the major phases detected in XRD analysis. For example, if NiO was one of the major phases, then the stability range should start at 200°C. Likewise, if there were any nickel borides in the final product, then the inner temperature of the selected zone should be at least 1050°C.

The distribution of thermal gradients for RUN 2 was also calculated using COMSOL Multiphysics® 5.2[20] and was given in the online supplementary material in Fig. S6. For the physics, a module titled "Heat Transfer Module-Joule heating" was selected. The furnace current–voltage characteristics were introduced into the model. On the other hand, the electrical conductivity (σ) was evaluated using various electrical resistance values obtained from the report of Keem and Honig.[21] The electrical conductivity (σ) was introduced as a function of temperature: $2 \times 10^8 \times T^6 - 7 \times 10^9 \times T^5 + 9 \times 10^{10} \times T^4 - 6 \times 10^{11} \times T^3 + 2 \times 10^{12} \times T^2 - 3 \times 10^{12} \times T + 2 \times 10^{12}$ (S/m). The thermal conductivity (k) value of the bulk material was evaluated using a temperature-dependent piecewise formula: $25.53808 - 0.04838285 \times T + 3.825482 \times 10^{-5} \times T^2 - 1.043009 \times 10^{-8} \times T^3$ (W/m K). As seen in the online supplementary material in Fig. S6, the hottest zone of the furnace is near the bottom electrode. The maximum temperature of the furnace could be 1670°C. The nickel borides can only be formed in the hottest zone and around the electrodes. This projection could not give the heat transferred by the hot gasses. The arc was modeled using the power and energy consumption data recorded during the process. The change in voltage, current, and power values collected during both preheating and reduction-melting stages is given in the online supplementary material in Fig. S7. The generation of arc and simulation of the thermal gradients were calculated as a result of these values.

Similar reactions and phases were achieved in the reaction zones between 0 mm and 600 mm for all experiments. The list of possible reactions and phases detected by XRD analysis is given in Table III.

Calculation of energy-balance can only be theoretically applied on the possible reactions. Enthalpy values of the raw materials were calculated using the "Reaction" module of FactSage™ 6.4. The results of chemical analysis for each raw material were used, and the volatile materials in charcoal and wood chips were assumed as moisture (H_2O). The standard enthalpy changes (ΔH°_{298K}) of the input materials were 1764.3 kJ/kg granulated boric acid, 332.9 kJ/kg technical grade nickel oxide, 620.7 kJ/kg charcoal #2, and 1425.2 kJ/kg wood chips, respectively.

To calculate the energy balance, the compounds and their compositions must be given for both input and output streams. In RUN 2, 100 kg of the initial mixture was used in a 900-mm-deep furnace. If we assume that the distribution of the initial mixture was homogenous through the furnace, then every 10 mm thickness zone of the furnace has 1.111 kg of initial mixtures. The value of standard enthalpy changes (ΔH°_{298K}) of the initial mixture in each 10 mm thickness was found to be 1199.7 kJ.

The compounds and their compositions in the output stream were measured via XRD analysis and the Rietveld refinement technique. PANalytical X'pert Highscore^{+} software with ICDD and ICSD databases were used to detect the possible phases and realize Rietveld refinement in default mode. Even though the relative intensities of the products were insufficient for complete Rietveld refinement, the relative ratios of the major phases were calculated. Rietveld refinement was realized in Automatic Mode via an available background method with the Pseudo Voigt profile function having a profile base width of 4.00. The refining of parameters (overall B and profile parameters) of each phase were made by manually until values of the agreement indices (R expected, R profile, Weighted R profile, and Goodness of fit) become acceptable. The results of Rietveld refinement are given in the online supplementary material in Table SIV. As a result of the amorphous phase contents in the by-products, the calculations for total material and energy balance were not applicable in this system. Nevertheless, an approach based on the nickel-containing compounds could be projected for the material balance.

The XRD results (Fig. 2) showed four nickel-containing compounds (NiO, Ni, Ni_2B, and NiB) were in the by-products. Technical grade nickel oxide is the only nickel source in the initial mixtures, and NiO is 99.0% pure. Material balance calculations were done with Eqs. 1c, 6a, and 6b, where the evaporation of the nickel-based compounds was neglected. As mentioned earlier, we assumed that there were 1.111 kg of initial mixtures in every zone with a thickness of 10 mm (RUN 2). For 1.111 kg of initial mixtures with a NiO content of 315.7 g (1.111 × 28.7% × 99% purity; approximately 4.23 mol), 4.23 mol of NiO were partly reduced and Ni, Ni_2B, and NiB were formed. The material balance details of nickel-containing sources are given in the online supplementary material in Table SV.

The energy values required for reducing NiO are also given in the online supplementary material in Table SV. Because of the higher temperatures and higher energy requirement of Eq. 6a relative to Eqs. 1c and 6b, the highest energy requirement values were observed at the bottom of the furnace. The standard enthalpy changes (ΔH°_{298K}) of Eqs. 1c, 6a, and 6b were −43.26, +380.43, and +159.95 kJ/mol NiO, respectively. The reduction of NiO to produce NiB requires higher energy than for producing Ni_2B. The overall energy requirement, based on nickel sources, for processing RUN 2 was calculated to be 18.56 MJ for 100 kg of the initial mixtures. The heat transferred via off-gasses was 34.70 MJ for the 100 kg of starting material. The energy of off-gasses was sufficient for total dehydration of H_3BO_3 into B_2O_3 (ΔH°_{298K} for Eq. 2c is 25.72 kJ/mol H_3BO_3) and reduction of NiO into Ni-based compounds.

Because the melting was only occurred in the lower part of the furnace, the Ni and B efficiencies were found to be minimal. The Ni recovery values were 50.0% in RUN 1, 30.2% in RUN 2, 46.0% in RUN 3, and 40.2% in RUN 4, respectively. The B recoveries were 20.3%, 19.3%, 29.2%, and 22.5%, respectively. Recovery values were calculated based on the chemical compositions of initial mixtures and master alloys obtained by tapping. For RUN 2, the total amount of Ni in the initial mixture was 22.326 kg (28.7 kg of technical grade nickel oxide × 99% × 58.69 g Ni per 74,69 g NiO), and the total amount of Ni in the master alloy was 6.73 kg (8.1 kg of master alloys × 83.11% Ni). By dividing 6.73 into 22.326, the nickel recovery values were found to be 30.2%. If we consider the amount of the reduced materials received in each zone (Table SV in the online supplementary material), then the total nickel recovery approached 55.81% (6.73 kg Ni in master alloy + 3.68 kg as metallic Ni + 0.99 kg Ni in Ni_2B + 0.89 kg Ni in NiB). Similarly, the total boron recovery values were recalculated to be 23.5% for RUN 2.

CONCLUSION

- Nickel-boron alloys were produced within the limitation values of the ASTM A323-05 ferroboron standard specification via a DC electric arc furnace starting from mixtures of boric acid, nickel oxide, charcoal, and wood chips.
- Depending on the consumed power-to-weight ratios of the raw materials, raw mixtures with lower fixed carbon and higher ash-containing charcoal required higher energy for reduction.
- The lowest electrode consumption rate was found with the highest fixed carbon-containing charcoal.
- The final alloys had a boron content of 9.9–14.8% by mass. The highest boron contents were reached when the lowest fixed carbon and the highest ash-containing charcoal were used.
- The XRD analysis showed that the phases detected in the final alloys were matched with the expected phases seen in the binary phase diagram.

- The XRD results showed that the Ni-B phases started to form under 600 mm depth, especially in the area under the top electrode.
- The detected phases and their possible reactions were also predicted as a result of the XRD results with thermochemical and physics-based modeling programs. The possible reactions were investigated, and their temperature and energy requirement values were detailed.
- The material and energy balances were calculated depending on the XRD Rietveld refinement results.

ACKNOWLEDGEMENTS

The authors thank Sentes-BIR and ITU-BAP (Istanbul Technical University, Office of Scientific Researches Projects) for financial support of this study. The authors thank Alper Kelesoglu (Yalova University) for assistance in COMSOL modeling and Zehra Inci Kol for assistance in chemical analysis.

ELECTRONIC SUPPLEMENTARY MATERIAL

The online version of this article (doi:10.1007/s11837-017-2439-y) contains supplementary material, which is available to authorized users.

REFERENCES

1. J.R. Davis, *ASM Specialty Handbook: Nickel, Cobalt, and Their Alloys* (Materials Park: ASM International, 2000), pp. 1–124.
2. R.C. Reed, *The Superalloys: Fundamentals and Applications* (Cambridge: Cambridge University Press, 2006), pp. 1–32.
3. V. Vitry, A.F. Kanta, and F. Delaunois, *Surf. Coat. Technol.* 206, 1879 (2011).
4. A.J. Frierdich, C.E. Joseph, and T.J. Strathmann, *Appl. Catal. B* 90, 175 (2009).
5. V.I. Balakai, V.V. Ivanov, I.V. Balakai, and A.V. Arzumanova, *Russ. J. Appl. Chem.* 82, 851 (2009).
6. I. Rajagopal, *Bull. Mater. Sci.* 5, 323 (1983).
7. V. Vitry, A.F. Kanta, and F. Delaunois, *Mater. Des.* 39, 269 (2012).
8. C.R. Pichard, Z. Bouhala, A.J. Tosser, A. Rashid, and J. Flechon, *J. Mater. Sci.* 20, 3305 (1985).
9. I.M. Fedorchenko, Y.A. Guslienko, and A.P. Epik, *Powder Metall. Metall. Ceram.* 11, 626 (1972).
10. F. Delaunois and P. Lienard, *Surf. Coat. Technol.* 160, 239 (2002).
11. Z.C. Wang, F. Jia, L. Yu, Z.B. Qi, Y. Tang, and G.L. Song, *Surf. Coat. Technol.* 206, 3676 (2012).
12. A. Corrias, G. Ennas, A. Musinu, G. Paschina, and D. Zedda, *J. Non Cryst. Solids* 192, 565 (1995).
13. V.I. Fadeeva, L.M. Kubalova, and I.A. Sviridov, *Steel Trans.* 41, 451 (2011).
14. J. Peng, R. He, M. Tan, Y. Dou, Z. Wang, G.Z. Chen, and X. Jin, *J. Electrochem. Soc.* 162, H271 (2015).
15. S.M. Nekhamin, A.G. Lunin, M.M. Krutyanskii, and A.K. Filippov, *Refract. Ind. Ceram.* 46, 37 (2005).
16. R.T. Jones, *Celebrating the Megascale: Proceedings of the Extraction and Processing Division Symposium on Pyrometallurgy in Honor of David GC Robertson*, eds. P.J. Mackey, E.J. Grimsey, R.T. Jones, and G.A. Brooks (Hoboken: Wiley, 2014), pp. 16–20.
17. R. Hahn, H.J. Retelsdorf, R. Fichte, and S. Sattelberger, U.S. Patent 4623386 (1986).
18. O. Yücel, F. Cinar, O. Addemir, and A. Tekin, *High Temp. Mater. Proc.* 15, 103 (1996).
19. C.W. Bale, et al., *Calphad* 33, 295 (2009).
20. E.J. Dickinson, H. Ekström, and E. Fontes, *Electrochem. Commun.* 40, 71 (2014).
21. J.E. Keem and J.M. Honig, *Selected Electrical and Thermal Properties of Undoped Nickel Oxide* (Lafayette: CINDAS, 1978), pp. 1–78.